Optical fiber sensor based on oblique angle deposition

Sasani Jayawardhana,[1,*] Gorgi Kostovski,[2] Alex P. Mazzolini,[1] and Paul R. Stoddart[1]

[1]Faculty of Engineering and Industrial Sciences, Swinburne University of Technology, Mail H38, P.O. Box 218, Hawthorn, Victoria 3122, Australia

[2]Platform Technologies Research Institute, Microplatforms Research Group, School of Electrical and Computer Engineering, RMIT University, Melbourne, Victoria 3001, Australia

*Corresponding author: sjayawardhana@swin.edu.au

Received 7 September 2010; revised 29 October 2010; accepted 16 November 2010; posted 17 November 2010 (Doc. ID 134394); published 6 January 2011

The technique of oblique angle deposition has been extended to the fabrication of nanostructured metal coatings on the tips of standard silica optical fibers by thermal evaporation. The coatings are initiated as metal island films, which grow into extended rodlike structures as the deposition continues. The nanorod coatings demonstrate excellent surface-enhanced Raman scattering performance with variability of less than 10% as shown by direct measurements off the fiber tip with thiophenol as a test analyte. However, in the remote sensing configuration, the nanorod structures perform no better than thin metal island films. This appears to be mainly due to reduced transmission when nanorod lengths exceed ~100 nm. Moreover, the variability of remote measurements is increased to 18%. This is believed to be due to variations in coupling efficiency.

OCIS codes: 240.6680, 280.4788, 060.2370, 280.0280, 300.6450, 220.4241.

1. Introduction

Surface-enhanced Raman scattering (SERS) has many potential applications in trace-level chemical and biological sensing due to its sensitivity and specificity [1–3]. The relaxed requirements on sample pretreatment or labeling and the ability to investigate small sample sizes under ambient conditions are attractive features that could potentially enable real time measurements.

The technique relies on the adsorption or close proximity of target molecules to a nanostructured metal surface. The topography of the nanostructured surface is fundamental in producing high scattering enhancement and is mainly attributed to the electromagnetic effect, which is a manifestation of localized surface plasmon fields that are excited by the incident light [4]. This effect can lead to enhanced sensitivities of around a millionfold compared to traditional Raman spectroscopy. Substrates can be tuned to a particular plasmon resonance as required, which provides great flexibility in sensing applications [5]. There can also be a contribution to the enhancement from a charge-transfer mechanism [6], but this is generally analyte specific and significantly weaker than the dominant electromagnetic effect.

Despite its many advantages, this technique is not without its challenges. Producing a robust, inexpensive substrate with high enhancement and good repeatability has been an ongoing issue. Over the years numerous methods have been utilized to fabricate SERS-active surfaces on planar substrates such as glass slides [7–9]. To date these experimental techniques have tended to be limited to laboratory research applications.

Optical fibers provide an excellent alternative platform for SERS sensing applications because they allow for *in situ* monitoring of small samples by acting as an "optrode" sensor [10]. Together with the chemical, thermal, and electrical passivity of silica optical fibers, this platform can be used for remote and *in vivo* sensing applications and in hazardous environments. A number of optical fiber SERS probes, which gather scattered light from the sample, have been reported in the literature, but these require

0003-6935/11/020155-08$15.00/0

an external source to deliver the excitation [11,12]. The optrode geometry exploits the bidirectional capability of the optical fiber to guide both the exciting and the scattered radiation through the fiber [13]. This requires fabricating the SERS sensing element on the distal end of the fiber. Given the microscopic diameter of the fiber tip, typically 125 μm, the number of fabrication techniques that can be feasibly employed for this task are limited.

White *et al.* fabricated a SERS optrode by chemically etching the tip of a drawn down optical fiber bundle [14]. Recent work by Guieu *et al.* took this a step further to show that a preferentially etched fiber bundle can be used for localized SERS measurements [15]. However, this technique not only requires specialized imaging fibers but also is susceptible to issues associated with dopant diffusion [16]. A nanoparticle-based SERS fiber probe has been attempted by Polwart *et al.* This probe relies on the aggregation of silver nanoparticles on the tip of a fiber [17]. Although this stochastic fabrication approach provided promising reproducibility (~10% variability within a batch), the robustness of the sensor remained a concern. The immobilization of nanoparticles in both air- and liquid-filled photonic crystal fibers (PCF) has been reported as promising for SERS sensors [18–20]. Although PCFs are becoming increasingly popular for their capabilities, the cost associated with their manufacture still remains prohibitively high.

Recently, e-beam lithography has been used to fabricate a nanoantenna array on a standard silicon substrate, which was then transferred onto the end facet of an optical fiber by a decal transfer method [21]. A similar approach was demonstrated by Kostovski *et al.* in transferring a naturally occurring cicada wing nanostructure onto a fiber tip by using an elastomeric mold [22]. This approach has great potential for being extended to high-throughput fabrication. An alternative technique is thin-film deposition using either thermal or electron-beam (e-beam) evaporation. This technique has been shown to be a very convenient way of constructing an SERS substrate on a fiber tip [23,24]. Despite the low enhancement and poor repeatability, thin-film deposition has been used by Scaffidi *et al.* to demonstrate the ability to detect local pH changes in biological cells without inducing apoptotic response of the cells [25].

Relatively large SERS enhancement factors have been reported for e-beam evaporated nanorod films prepared by oblique angle deposition (OAD) [26,27]. Although the enhancement appears to rise as the length of the nanorods increases, the detailed mechanism behind this high enhancement is still not completely understood [28]. OAD provides a relatively convenient and inexpensive way of producing SERS substrates using electron-beam evaporation, not only on a planar surface but also on cylindrical objects [29] and on the distal end of optical fibers [30]. The work presented here demonstrates that the production of SERS-active nanorods by the OAD technique can be further simplified by using the more accessible thermal evaporation technique and provides a systematic characterization of the resulting optical fiber sensor. The viability and other challenges associated with the fabrication and application of an optical fiber chemical sensor prepared by thermal OAD are then discussed in Section 4.

2. Experiment

A. Materials

Silver (99.95%, Goodfellow) and chromium (99.99%, ProSciTech) were purchased and used without further treatment. The planar substrates used to prepare nanorods were silicon wafers with a thermally grown 300 nm thermal oxide layer (University Wafer). This oxide layer was expected to provide similar surface characteristics to that of a silica fiber optic end face for characterization purposes. Standard silica fibers (Corning) with a 62.5/125 μm core/cladding diameter and a numerical aperture (NA) of 0.272 were chosen for the fabrication of the SERS optrode. A 10 mM ethanolic solution was prepared from thiophenol (99%+, Sigma–Aldrich) and used as the test analyte for the SERS characterization of the substrates. Thiophenol is commonly used as a test analyte for SERS as it provides a strong signal and is expected to consistently form a self-assembled monolayer [31]. All solvents were 99% or higher purity and were used without further treatment.

B. Instrumentation

Silver nanorod films were fabricated by the OAD technique using an Emitech K975X Turbo Evaporator. In order to ensure repeatability of fabrication, the evaporator was modified by incorporating a custom-made evaporation source holder to fix the filament position with respect to the sample. The same apparatus was used in a sputtering mode to deposit a chromium adhesion layer. The evaporation angle is defined in Fig. 1. The quartz crystal monitor was used to measure the thickness of the normally deposited film thickness on the crystal and is described as the "nominal thickness." It was not possible to control the substrate temperature in this system; thus the deposition rate was restricted to 0.05 nm s^{-1} in order to reduce radiant heating of the substrate by the source.

SERS spectra were collected using a Horiba Jobin–Yvon modular Raman microscope and Triax 320 spectrometer fitted with a thermoelectrically cooled CCD. The samples were excited using a fiber-coupled diode-pumped solid state laser with a wavelength of 532 nm and 1 mW power at the sample. A 50× objective with a 0.5 NA was used for all data collection.

Scanning electron microscope (SEM) images were obtained using a Nova NanoSEM in low vacuum mode to reduce sample charging effects. For the "through fiber" transmission measurements, a fiber-coupled halogen lamp (HL-2000 Ocean Optics) was used as the source along with an Ocean Optics Red Tide (USB650) spectrometer as the detector element.

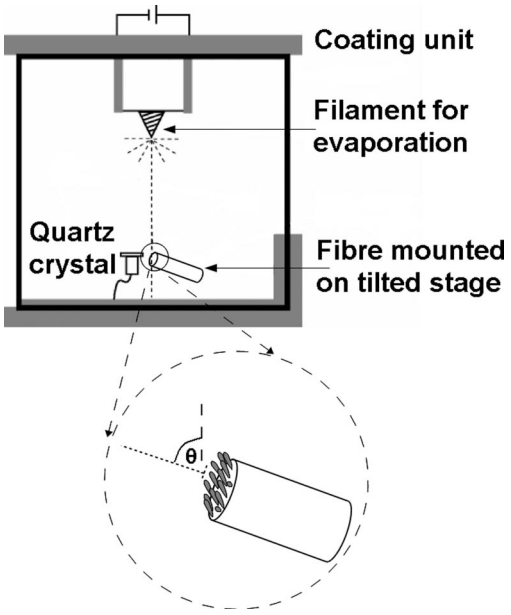

Fig. 1. Experimental setup for oblique angle deposition. The inset shows the growth of nanorods on the fiber tip. The angle between the sample normal and the direction of vapor flux is depicted as θ.

C. Sample Preparation

Silicon wafers were diced into chips of 4 mm × 15 mm using a dicing saw (Disco DAD 321). The samples were thoroughly cleaned with acetone to remove any debris and any trace of the protective photoresist that was applied during the dicing process. The optical fibers were stripped, cleaned with acetone, and cleaved at both ends to produce samples of 25 mm length before coating. These were used for both direct and remote measurement geometries.

Prior to silver deposition a 2 nm layer of chromium was sputtered onto both the silicon wafer sample surfaces and the optical fiber tips to aid in the adhesion of silver to the silica surface. The sputtering was carried out under normal incidence with substrate rotation. Both types of sample were mounted at an oblique angle to the vapor flux by tilting the sample stage in the evaporation unit. In the case of the fiber sections, the distal ends of the fibers were covered with a shield to prevent any silver being deposited.

The substrates were then soaked in a 10 mM solution of thiophenol for 10 min, rinsed with ethanol, and interrogated for SERS. Spectra were collected directly off the coated surface of the fiber and remotely by coupling the excitation and backscattered Raman signal through the optical fiber waveguide (Fig. 2). The direct signal collection employs a high-NA objective (0.5) and the collected Raman-scattered light can be assumed to be limited by the signal gathering capability of the objective. However, for the remote signal collection, the scattered light is guided through the fiber probe prior to entering the objective and is thus limited by the NA of the fiber probe (0.272), which is smaller than the NA of the objective in use. In order to carry out a systematic analysis of the

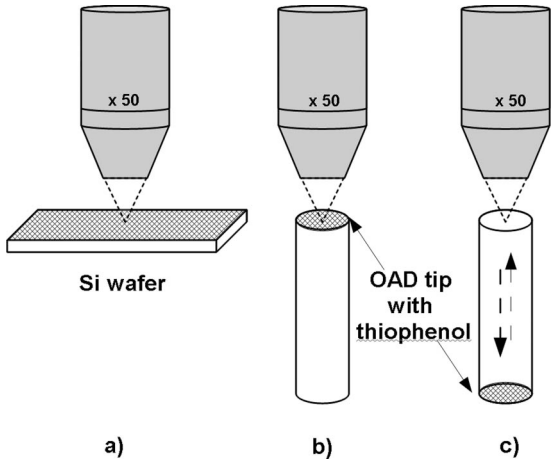

Fig. 2. SERS measurement methods for a) silicon wafer, b) optical fiber in the direct sensing geometry, and c) optical fiber in the remote sensing geometry.

SERS capabilities of the two geometries, these differences in optics need to be taken into account. A signal integration time of 5 s (with three averages) was employed to collect the spectra. For comparison purposes all measurements have been normalized to take into account variations in the incident laser power, the signal acquisition time, and the solid angle of signal collection (counts.s^{-1}.mW^{-1}.sr^{-1}).

The NA of the optical fiber facet at the silver OAD coating was not adjusted for the refractive index of silver because the scattering is considered to be a near-field process occurring at the silver surface. Once the scattered light enters the far field, the propagation of light within the optical fiber will be determined by the properties of the optical fiber.

D. Transmission Measurements

For transmission measurements, fiber samples of roughly 2 m length were used. The fibers were cleaved at both ends and the silver nanorod films were fabricated on one end as described earlier. The remote end was later cleaved to ensure a clean surface and coupled into the measurement setup as shown in Fig. 3. Five samples of each OAD film thickness were averaged to arrive at the transmission measurements shown in this paper.

The white light from the halogen light source was sent through the microscope and coupled into the cleaved end of the fiber. In order to couple the transmitted light into the fiber-coupled spectrometer, the OAD coated fiber tip was mounted in a temporary connector. The positioning of the coated tip was checked under a microscope to ensure that the nanostructured surface was protected within the ferrule of the temporary connector. To separate the transmission spectrum of the film from that of the fiber, all spectra collected were normalized against a spectrum from a fiber of the same length that was simply cleaved at both ends. It was important to align the fiber samples in the ferrule in a consistent fashion because the alignment plays a significant factor in determining

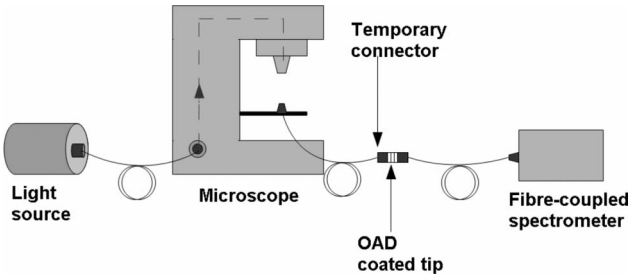

Fig. 3. Experimental setup for the transmission measurements through the fiber with the OAD silver coating. The white light was sent through a microscope to control the intensity coupled into the fiber sample.

coupling efficiency. This was done by placing the fiber in the ferrule under a microscope and adjusting the longitudinal position of the fiber end face until it was visually in plane with the ferrule surface. The repeatability of the alignment procedure was determined to have an uncertainty of ± 0.05 absorbance units.

3. Results

Figure 4(a) shows a typical thiophenol SERS spectrum. For purposes of comparison, the peak heights of the four main thiophenol peaks at 1000, 1021, 1072, and 1573 cm^{-1} were averaged to arrive at a single numerical value for each measurement. This value has a strong correlation to the area under the four peaks (coefficient of correlation $r = 0.978$).

A. Angle Optimization for SERS

Nanorod growth is believed to occur at highly oblique deposition angles due to an initial seeding and self-shadowing mechanism [32]. OAD was carried out on several silicon wafer samples with different deposition angles to ascertain the optimum angle for SERS performance in this thermal evaporation system. All samples were coated with a nominal silver thickness of 80 nm as recorded on the quartz crystal microbalance. Figure 4(b) presents a subset of the angles tested. Deposition angles outside the shown range generated even lower signal intensities. This demonstrates that the peak SERS signals were generated by a coating angle of $\theta = 86°$. This has been further confirmed by similar tests done on samples with a 200 nm nominal thickness (data not shown). This angle is in agreement with published results for an e-beam deposition system [26]. Liu *et al.* [33] presented a thorough characterization of the angle, rod length, and SERS that demonstrates that the optimum angle could shift as the nanorod length increases. Nevertheless, the OAD films that were used in this work were considerably thinner than those reported and can be considered to maintain the optimum angle at 86° throughout the increase in thickness.

B. Coating Structure and Thickness

Figure 5 presents SEM images of nanorod growth in top view and cross section. These rod structures were fabricated on planar silicon substrates and were cleaved to reveal the cross section. The planar substrates were chosen for the imaging because longitudinal cleaving of the optical fiber samples was not a viable option. It is assumed that the nanorod structures grown on the face of the fibers follow a similar trend to those on the planar substrate because of their similar appearance (top view) and comparable SERS performance. In both cases the nanorods start to form around a nominal thickness of 300 nm.

While silver was deposited in steps of 100 up to 600 nm as recorded on the quartz crystal microbalance, the actual average nanorod lengths were determined from the SEM images to be 31 ± 5, 90 ± 11, 119 ± 16, 208 ± 23, 260 ± 28, and 329 ± 21 nm. There appears to be a reasonably linear relationship between the nominal thickness and the actual nanorod length, which is shown in Fig. 6. The nanorod inclination angle with respect to the substrate surface appears to decrease slightly as the thickness increases. Figure 5(a) could not be assigned an inclination angle due to the rounded nature of the metal islands. The angles for the rest of the nanorods were

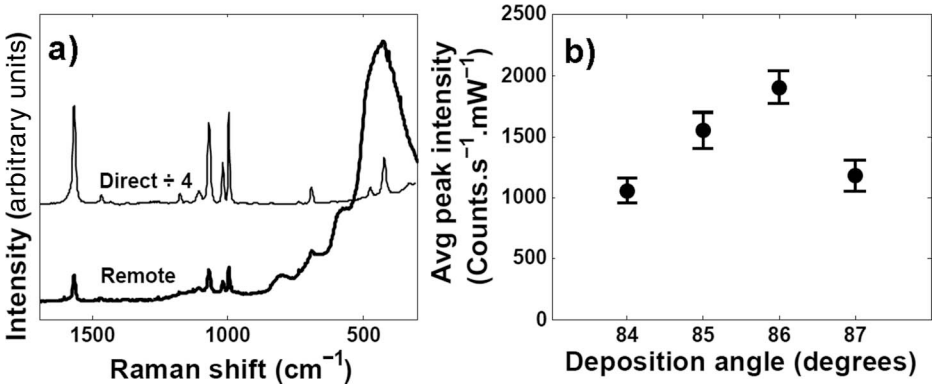

Fig. 4. a) Typical thiophenol SERS spectra from the direct and remote measurements for a deposition angle of 86°. The large background of ~500 cm^{-1} in the remote geometry is due to Raman scattering in the silica optical fiber. b) Variation in the average peak intensity of the four main thiophenol peaks as a function of the vapor deposition angle θ. The error bars represent the standard deviation across ten measurements.

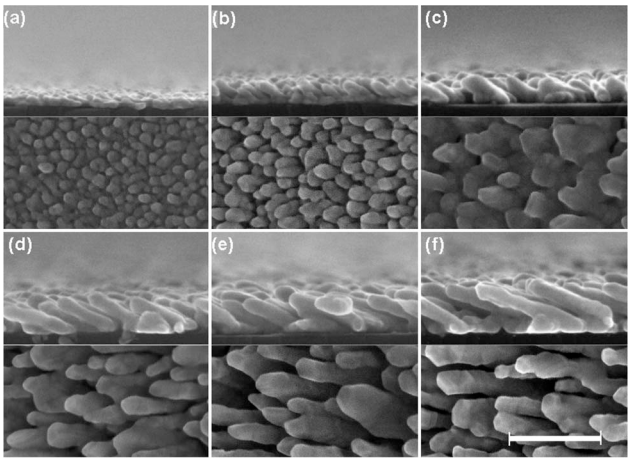

Fig. 5. SEM images of the silver nanorod formation on a silicon wafer, cross section and top-down view with nominal thicknesses of (a) 100, (b) 200, (c) 300, (d) 400, (e) 500, and (f) 600 nm, with the scale bar showing 200 nm. The vapor deposition angle was maintained at 86°.

estimated to be $39 \pm 2°$, $39 \pm 2°$, $30 \pm 1°$, $29 \pm 1°$, and $26 \pm 1°$, in order of increasing thickness.

The nanorod diameter appears to increase linearly with nanorod length, which is consistent with the results reported by Liu *et al.* [33]. However, it should be noted that the nanorod diameter differs in the two viewing directions shown in Fig. 5. The nonuniformity of the diameter along the rod and the wide distribution of sizes across a sample make it difficult to quantify this parameter more precisely. The number of nanorods per unit area appears to drop off as the film increases in thickness because of coalescence of neighboring islands.

C. Thickness Optimization for SERS

The variation of the average SERS peak intensity with increasing metal deposition thickness is shown in Fig. 7. Each data point is an average of ten measurements per sample across five samples. All measurements have been normalized for the incident laser power, the signal acquisition time, and the solid angle of signal collection.

The direct signal increases with increasing metal thickness and peaks around a rod height of 260 ± 28 nm, after which it exhibits a downward

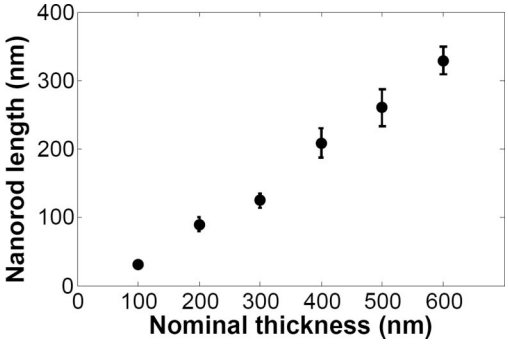

Fig. 6. Relationship between the nominal thickness as recorded on the quartz crystal microbalance and the actual nanorod length as estimated using the SEM images of Fig. 5.

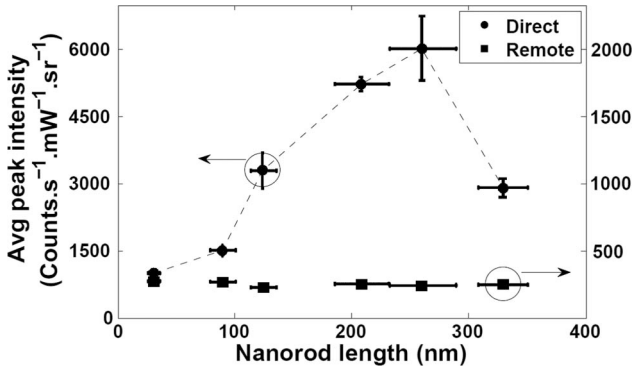

Fig. 7. Average SERS intensity of the fiber samples in remote and direct interrogation is plotted against nanorod length. Each data point was an average of 10 measurements per fiber across five fibers.

trend. Previous work by Driskell *et al.* [27] demonstrated that an increase in the SERS enhancement factor is achieved up to a nanorod length of 868 nm and, thus, concluded that the optimum geometry of the SERS nanostructure overrides any further increase in surface area. In the work presented here it is possible that the optimum geometry is achieved at a nanorod length of 260 nm. However there could also be other factors such as rising temperature inside the vacuum chamber affecting the silver surface, particularly for the thicker films. Although further investigation of the nanorod geometry would be of interest for the direct SERS measurements, the remote measurements are more relevant for the purpose of developing a fiber optrode.

There is a significant difference between the SERS signals collected directly off the tip of the fiber and remotely through the fiber. The remote measurement exhibits an approximately constant intensity response irrespective of the deposition thickness. For thin coatings, these remote measurements are ~25% of the direct measurement, whereas relative to the optimum nanorod length of 260 nm, the signal is ~5%. The reduced coupling efficiency of the laser light through the fiber means that in remote interrogation, the sample excitation intensity is lower than that of the direct interrogation and would account for a portion of the drop in intensity. This factor cannot be reliably quantified for the short lengths of fiber that were used but is estimated to be approximately 20–25%. Other possible explanations for the reduction in performance are discussed in Section 4.

D. Transmission Measurements

A custom-made transmission measurement setup was built using a fiber-coupled halogen light source and a detector as shown in Fig. 3. Transmission spectra from fibers with different coating thicknesses are shown in Fig. 8. Absorbance values were calculated according to

$$A_\lambda = -\log_{10}\left(\frac{I_\lambda - D_\lambda}{I_0 - D_\lambda}\right),$$

where A_λ is the absorbance at wavelength λ, I_λ is the measured intensity of the light at wavelength λ, I_0 is the intensity of the reference beam at wavelength λ, and D_λ is the intensity of the dark spectrum at wavelength λ.

Figure 8 depicts the broadband transmission properties of the thermal OAD films in the visible–near-infrared wavelength range. Except for the two thinnest films, it is interesting to note the absence of a clearly defined plasmon absorption peak. The transmission spectra indicate that the high reflectivity of the thicker coatings reduces the transmission and therefore may limit the SERS signal collected through the remote geometry.

E. Repeatability

The repeatability of the SERS substrates can be classified in three different ways: (i) the repeatability within a single sample, (ii) the repeatability across samples within a single fabrication run, and (iii) the repeatability across different fabrication runs.

For the assessment of repeatability, ten measurements were performed at different points on each of five fiber samples per coating run. The estimated variability across a single sample was $<10\%$ based on relative standard deviation (RSD), which is among the best reported for OAD films [27]. Thin island films are known to exhibit an inherent degree of variability due to the random nature of island formation, but there could also be a contribution by the substrate cleaning process. Better results might be obtainable with seeded growth, where a prepatterned sample is used for the rod growth [34]. The variability across samples fabricated in a single batch was also estimated to be $<10\%$ of the mean value of each sample.

To determine the repeatability between batches, eight deposition runs of 400 nm nominal thickness were considered. The RSD across these samples was calculated to be $<5\%$, which is a significantly lower value than has been reported elsewhere [27]. In order to ensure this level of repeatability over different fabrication runs, it was necessary to maintain the deposition rate at a constant and low value. Because of the nature of the coating unit, it was found that the deposition rate influenced the temperature inside the chamber and thus played a major role in the fabrication of the nanorods. A high deposition rate requires a high electrical current through the evaporation source. It was observed that a relatively high current (11 A) increased the temperature inside the chamber to over 80 °C within a 4 min time period, whereas a lower current (8 A), which was just enough to start and maintain the evaporation process, did not raise the chamber temperature above 38 °C even after 5 min. This observation is believed to be a consequence of the fact that the radiant heat emanating from the source scales to the fourth power of temperature. Increasing substrate temperature is known to increase adatom and vacancy diffusion rates on silver surfaces, which in turn accelerates the coalescence of neighboring structures. Thus the increase in temperature inside the chamber could have contributed to structural changes in the silver film, resulting in a high level of variation in signal across different fabrication runs [35].

The variability of the signals collected through the fiber tend to be rather higher (RSD $<18\%$) than those collected off the tip of the fiber (RSD $<10\%$). The variability in coupling efficiency as well as cleaving defects can play a role in contributing to the variation.

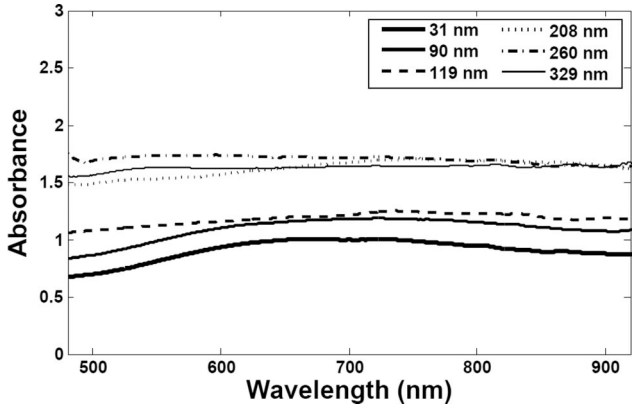

Fig. 8. Absorbance profile for different nanorod lengths on optical fiber tips. A Savitzky–Golay filter has been used to smooth the data.

4. Discussion and Conclusion

Oblique angle deposition has proved to be an attractive method for the fabrication of SERS substrates, not only because of the high enhancement and high repeatability of the substrates, but because of the relative ease and low cost associated with this fabrication method. For optical fiber SERS probes, thermal OAD films provide excellent SERS substrates when measured directly but are relatively inefficient in the remote configuration.

Although the estimation of a SERS enhancement factor would be useful for comparison purposes, an assessment of the number of molecules being excited is not straightforward. The substrates used in this work do not provide a conducting surface for traditional electrochemical techniques to be employed for estimating the surface area illuminated by the laser spot. Further, care is needed to ensure that the incorporation of a conducting layer does not change the kinetics of the coating process, thereby possibly modifying the film structure and SERS performance [36]. While the overall magnitude of the SERS signal is of primary importance in the current context of developing a practical optical fiber SERS sensor, further work would be needed in order to obtain an accurate enhancement figure.

The thin OAD films shown in Fig. 5(a) provide metal island film structures rather than nanorods. In this thin film regime the SERS performance appears to be similar to the metal island films on optical fibers reported by Viets and Hill [23]. However, the optimum SERS performance of OAD lies in thicker films, which cannot be accessed for fiber probes. According to

Fig. 8, the single pass transmission through thicker films appears to be heavily restricted. However, in SERS measurement in the remote geometry, the excitation light needs to travel through the OAD film to access the scattering analyte that's coated on the silver nanorods. The scattered radiation then needs to be collected back through the fiber, resulting in a double pass transmission through the OAD film. Although the far-field transmission cannot be directly applied to these results because of the near-field nature of the localized plasmon fields, it appears that the low transmission may partially account for poor performance through the fiber.

Therefore, optical fiber SERS probes require thin metal films with high transmission and high enhancement values in order to achieve better performance than metal island films. This could be satisfied by deriving the nanostructure from a transparent material, perhaps by roughening [24] or imprinting [22], followed by coating with a thin layer of metal. In the context of OAD, seeding of the nanorod growth may provide a means to control the surface coverage of the metal film and so enable higher transmission [37].

The poor performance of thicker films cannot be directly accounted for by the collection efficiency (NA) of the optical fiber probes. However, the correction for solid angle of signal collection is based on the assumption of an isotropic scattering distribution. In reality the scattering intensity distribution could be anisotropic, as has been demonstrated by several researchers [38,39]. In the latter work on nanorods [39] it was shown that the scattering intensity increases with angle from the incident beam up to a maximum scattering intensity at an angle of 45° to the substrate surface normal. This trend could help in explaining the more than proportional loss in signal due to a reduction of the NA from the direct collection (half angle 30°) to the remote collection (half angle 16°). However, a more detailed investigation is needed in order to verify this possibility.

It should be noted that thermally grown nanorod films can exhibit different structural and optical characteristics from those grown using e-beam deposition reported in the literature [26]. Conditions such as the degree of collimation of the vapor flux, grain size, kinetic energy of the vapor, surface diffusion, residual gas pressure, and temperature can all play a role in the growth of the film. Therefore the differences in the two methods as well as the equipment would determine the growth parameters of the OAD film.

This work was supported by the National Health and Medical Research Council through development grant 448610. The authors thank Paul Jones and his team at the Microelectronics and Materials Technology Centre at RMIT for their help with the sample preparation.

References

1. P. Etchegoin, R. C. Maher, L. F. Cohen, H. Hartigan, R. J. C. Brown, M. J. T. Milton, and J. C. Gallop, "New limits in ultrasensitive trace detection by surface enhanced Raman scattering (SERS)," Chem. Phys. Lett. **375**, 84–90 (2003).
2. J. Kneipp, B. Wittig, H. Bohr, and K. Kneipp, "Surface-enhanced Raman scattering: a new optical probe in molecular biophysics and biomedicine," Theor. Chem. Acc. **125**, 319–327 (2009).
3. C. L. Haynes, C. R. Yonzon, X. Y. Zhang, and R. P. Van Duyne, "Surface-enhanced Raman sensors: early history and the development of sensors for quantitative biowarfare agent and glucose detection," J. Raman Spectrosc. **36**, 471–484 (2005).
4. M. Moskovits, "Surface-enhanced Raman spectroscopy: a brief retrospective," J. Raman Spectrosc. **36**, 485–496 (2005).
5. R. Gupta, M. J. Dyer, and W. A. Weimer, "Preparation and characterization of surface plasmon resonance tunable gold and silver films," J. Appl. Phys. **92**, 5264–5271 (2002).
6. M. T. Sun, S. S. Liu, Z. P. Li, J. M. Duan, M. D. Chen, and H. X. Xu, "Direct visual evidence for the chemical mechanism of surface-enhanced resonance Raman scattering via charge transfer: (II) Binding-site and quantum-size effects," J. Raman Spectrosc. **40**, 1172–1177 (2009).
7. D. A. Stuart, J. M. Yuen, N. S. O. Lyandres, C. R. Yonzon, M. R. Glucksberg, J. T. Walsh, and R. P. Van Duyne, "In vivo glucose measurement by surface-enhanced Raman spectroscopy," Anal. Chem. **78**, 7211–7215 (2006).
8. D. S. Jung, Y. M. Lee, Y. Lee, N. H. Kim, K. Kim, and J. K. Lee, "Facile fabrication of large area nanostructures for efficient surface-enhanced Raman scattering," J. Mater. Chem. **16**, 3145–3149 (2006).
9. W. Yuan, H. P. Ho, R. K. Y. Lee, and S. K. Kong, "Surface-enhanced Raman scattering biosensor for DNA detection on nanoparticle island substrates," Appl. Opt. **48**, 4329–4337 (2009).
10. P. R. Stoddart and D. J. White, "Optical fibre SERS sensors," Anal. Bioanal. Chem. **394**, 1761–1774 (2009).
11. D. L. Stokes, Z. H. Chi, and T. Vo-Dinh, "Surface-enhanced-Raman-scattering-inducing nanoprobe for spectrochemical analysis," Appl. Spectrosc. **58**, 292–298 (2004).
12. J. M. Bello and T. Vo-Dinh, "Surface-enhanced Raman-scattering fiberoptic sensor," Appl. Spectrosc. **44**, 63–69 (1990).
13. D. L. Stokes and T. Vo-Dinh, "Development of an integrated single-fiber SERS sensor," Sens. Actuators B **69**, 28–36 (2000).
14. D. J. White, A. P. Mazzolini, and P. R. Stoddart, "Fabrication of a range of SERS substrates on nanostructured multicore optical fibres," J. Raman Spectrosc. **38**, 377–382 (2007).
15. V. Guieu, P. Garrigue, F. Lagugne-Labarthet, L. Servant, N. Sojic, and D. Talaga, "Remote surface enhanced Raman spectroscopy imaging via a nanostructured optical fiber bundle," Opt. Express **17**, 24030–24035 (2009).
16. D. J. White, A. P. Mazzolini, and P. R. Stoddart, "First-approximation simulation of dopant diffusion in nanostructured silica optical fibres," Photonics Nanostruct. **6**, 167–177 (2008).
17. E. Polwart, R. L. Keir, C. M. Davidson, W. E. Smith, and D. A. Sadler, "Novel SERS-active optical fibers prepared by the immobilization of silver colloidal particles," Appl. Spectrosc. **54**, 522–527 (2000).
18. M. K. K. Oo, Y. Han, J. Kanka, S. Sukhishvili, and H. Du, "Structure fits the purpose: photonic crystal fibers for evanescent-field surface-enhanced Raman spectroscopy," Opt. Lett. **35**, 466–468 (2010).

19. Y. Han, S. L. Tan, M. K. K. Oo, D. Pristinski, S. Sukhishvili, and H. Du, "Towards full-length accumulative surface-enhanced Raman scattering-active photonic crystal fibers," Adv. Mater. **22**, 2647–2651 (2010).
20. Y. Zhang, C. Shi, C. Gu, L. Seballos, and J. Z. Zhang, "Liquid core photonic crystal fiber sensor based on surface enhanced Raman scattering," Appl. Phys. Lett. **90**, 193504(2007).
21. E. J. Smythe, M. D. Dickey, J. M. Bao, G. M. Whitesides, and F. Capasso, "Optical antenna arrays on a fiber facet for in situ surface-enhanced Raman scattering detection," Nano Lett. **9**, 1132–1138 (2009).
22. G. Kostovski, D. J. White, A. Mitchell, M. W. Austin, and P. R. Stoddart, "Nanoimprinted optical fibres: Biotemplated nanostructures for SERS sensing," Biosens. Bioelectron. **24**, 1531–1535 (2009).
23. C. Viets and W. Hill, "Fibre-optic SERS sensors," Internet J. Vib. Spectrosc. **4** (2000), http://www.ijvs.com.
24. K. I. Mullen and K. T. Carron, "Surface-enhanced Raman spectroscopy with abrasively modified fiber optic probes," Anal. Chem. **63**, 2196–2199 (1991).
25. J. P. Scaffidi, M. K. Gregas, V. Seewaldt, and T. Vo-Dinh, "SERS-based plasmonic nanobiosensing in single living cells," Anal. Bioanal. Chem. **393**, 1135–1141 (2008).
26. S. B. Chaney, S. Shanmukh, R. A. Dluhy, and Y.-P. Zhao, "Aligned silver nanorod arrays produce high sensitivity surface-enhanced Raman spectroscopy substrates," Appl. Phys. Lett. **87**, 031908 (2005).
27. J. D. Driskell, S. Shanmukh, Y. Liu, S. B. Chaney, X. J. Tang, Y. P. Zhao, and R. A. Dluhy, "The use of aligned silver nanorod Arrays prepared by oblique angle deposition as surface enhanced Raman scattering substrates," J. Phys. Chem. C **112**, 895–901 (2008).
28. Y. J. Liu, Z. Y. Zhang, Q. Zhao, R. A. Dluhy, and Y. P. Zhao, "Surface enhanced Raman scattering from an Ag nanorod array substrate: the site dependent enhancement and layer absorbance effect," J. Phys. Chem. C **113**, 9664–9669 (2009).
29. J.-G. Fan and Y.-P. Zhao, "Direct deposition of aligned nanorod array onto cylindrical objects," J. Vac. Sci. Technol. B **23**, 947–953 (2005).
30. J. G. Fan, Y. J. Liu, and Y. P. Zhao, "Integrating aligned nanorod array onto optical fibers for SERS probes," Proc. SPIE **6327**, 63270R (2006).
31. M. A. Bryant and J. E. Pemberton, "Surface Raman-scattering of self-assembled monolayers formed from 1-alkanethiols at Ag," J. Am. Chem. Soc. **113**, 3629–3637 (1991).
32. J. Steele and M. Brett, "Nanostructure engineering in porous columnar thin films: recent advances," J. Mater. Sci.: Mater. Electron. **18**, 367–379 (2006).
33. Y. J. Liu, H. Y. Chu, and Y. P. Zhao, "Silver nanorod array substrates fabricated by oblique angle deposition: morphological, optical, and SERS characterizations," J. Phys. Chem. C **114**, 8176–8183 (2010).
34. M. O. Jensen and M. J. Brett, "Periodically structured glancing angle deposition thin films," IEEE Trans. Nanotechnol. **4**, 269–277 (2005).
35. K. Morgenstern, G. Rosenfeld, E. Laegsgaard, F. Besenbacher, and G. Comsa, "Measurement of energies controlling ripening and annealing on metal surfaces," Phys. Rev. Lett. **80**, 556–559 (1998).
36. Q. Zhou, Y. Liu, Y. He, Z. Zhang, and Y.-P. Zhao, "The effect of underlayer thin films on the surface-enhanced Raman scattering response of Ag nanorod substrates," Appl. Phys. Lett. **97**, 121902(2010).
37. Y. Zhao, D. Ye, G.-C. Wang, and T.-M. Lu, "Designing nanostructures by glancing angle deposition," Proc. SPIE **5219**, 59–73 (2003).
38. B. Pettinger, U. Wenning, and H. Wetzel, "Angular resolved Raman-spectra from pyridine adsorbed on silver electrodes," Chem. Phys. Lett. **67**, 192–196 (1979).
39. Y. J. Liu, J. G. Fan, Y. P. Zhao, S. Shanmukh, and R. A. Dluhy, "Angle dependent surface enhanced Raman scattering obtained from a Ag nanorod array substrate," Appl. Phys. Lett. **89**, 173134 (2006).